Eccentricity Analysis and Efficiency Estimation of 12/14 Hybrid Stator Pole Bearingless SRM

Zhenyao Xu, Jin-Woo Ahn

Kyungsung University, Busan, 608-736, Korea, zhenyao87@163.com

***Abstract*—The radial force to suspend the rotor in a constant air-gap for bearingless switched reluctance motor (BLSRM) is dependent on air-gap and force current. Due to the non-linear characteristic of inductance, the radial force is much affected by the rotor eccentricity. In order to keep constant air-gap of rotor, the nonlinear characteristics of eccentricity should be analyzed. Further, the auxiliary bearing is always used to restrict the maximum eccentricity of the rotor in industry. In this paper, the rotor eccentricity effect in the proposed 12/14 BLSRM is analyzed. Meanwhile, the efficiency of the 8/10 and proposed BLSRMs is estimated. The analysis results further verify the validity of the proposed BLSRM.**

I. INTRODUCTION

Switched reluctance motors (SRMs) have simple structure and inherent mechanical strength without rotor winding and permanent magnet, which make SRMs suitable for operating in harsh environments, e.g. high temperature and high speed applications [1-2]. Moreover, in SRM, a significant amount of magnetic attraction is generated in the radial direction, because switched reluctance motors generally have short air gap lengths in order to effectively produce rotational reluctance torque. It is quite possible to take advantage of this inherent large magnetic attraction for rotor shaft magnetic suspension. Therefore, SRMs could be a strong candidate for beringless motors.

Recently, several structures of bearingless switched reluctance motor (BLSRM) have been proposed [3-9]. But all of them are based on general SRM structure, the torque control is coupled with the suspending force control. A BLSRM with hybrid stator poles is proposed [1]. Compared with conventional BLSRM, the suspending force performance is improved, but in this structure, only half of the stator poles are used for the torque, output power density is very low. Moreover, in the motor long flux paths are present and flux reversal exists in the stator core, which increases the magneto motive force (MMF) requirements and leads to higher core losses.

To improve the performances of BLSRM, a novel 12/14 hybrid stator pole type BLSRM is proposed [10]. The proposed structure has separated torque and suspending force poles, the torque control can be decoupled from the suspending force control. Moreover, due to the short flux path without any reversal flux in the stator core, compared to the 8/10 hybrid stator pole type, the output torque is significantly improved and the air-gap is easier to control. But in this paper the effect of rotor eccentricity is not considered yet.

As is generally known, the rotor of the proposed BLSRM cannot be supported by mechanical bearing. So, the rotor can suffer displacement and eccentricity effects caused by a disturbance load and force. Rotor eccentricity, which changes rotor position in air gap, greatly influences the distribution of magnetic flux in air gap and causes a great variation in torque and force. Furthermore, the variations of torque and force may influence the suspension performance of BLSRM. In this paper, the eccentricity effect of proposed BLSRM is analyzed. Meanwhile, the efficiency of the proposed BLSRM is estimated. The validity of the proposed structure is verified by the analysis results.

II. A NOVEL 12/14 HYBRID STATOR POLE TYPE BLSRM

A. Structure of 12/14 BLSRM

A novel 12/14 hybrid stator pole type BLSRM with short flux paths and no flux reversal in the stator is proposed in Fig. 1. The proposed structure has separated torque and suspending force poles. Windings on the torque poles P_{A1}, P_{A2}, P_{A3} and P_{A4} are connected in series to construct phase A, and windings on the torque poles P_{B1}, P_{B2}, P_{B3} and P_{B4} are connected in series to construct phase B. The x-direction suspending force is generated by currents flowed in the suspending force poles P_{xp} and P_{xn}. Such as, the current i_{xp} in the stator pole P_{xp} generates positive x-direction suspending force, and the current i_{xn} in the stator pole P_{xn} can generate the negative x-direction suspending force. Similarly, the suspending forces for the y-direction can be generated by the

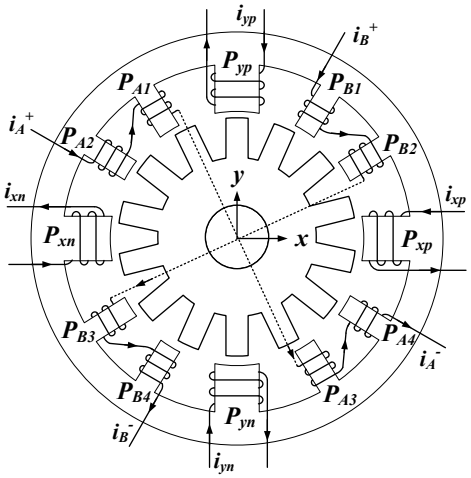

Figure 1. Basic structure of 12/14 BLSRM.

currents i_{yp} and i_{yn} which flow in suspending force poles P_{yp} and P_{yn}, respectively. Meanwhile, in order to get the continuous suspending force, the suspending force pole arc is selected not to be less than one-rotor pole pitch.

B. Torque and Suspending Force Model

Fig. 2 shows the attraction force produced by one stator and rotor poles. Because the magnetic flux passes through the overlapped area as well as the non-overlapped area due to fringing, the inductance of this pair of poles was modeled in [5] as,

$$L = \frac{\mu_0 N^2 L_{stk} r}{g}\left(\theta_o + K_f\right) \tag{1}$$

where, μ_0 is the permeability of the air, N is the number of coil turns, L_{stk} is the motor stack length, r is the rotor radius, g is the air gap length, K_f is a constant for the fringing inductance, θ_o and θ_{uo} are the overlapping and the non-overlapping angle, respectively.

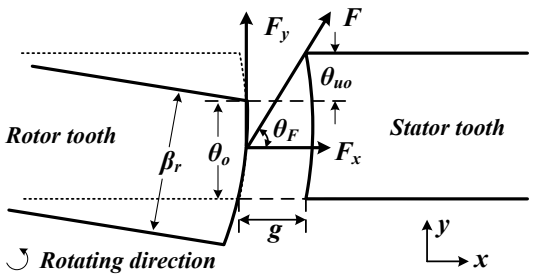

Figure 2. Attraction force produced by one stator and rotor poles.

From (1), the torque and radial force of the pair of poles can be approximately calculated as,

$$T = \frac{1}{2} i^2 \frac{dL}{d\theta} = \left(\frac{\mu_0 N^2 L_{stk} r i^2}{2g}\right) \cdot \frac{d\theta_o}{d\theta} \tag{2}$$

$$F = \frac{1}{2} i^2 \frac{dL}{dg} = \left(\frac{\mu_0 N^2 L_{stk} r i^2}{4g^2}\right) \cdot \left(\theta_o + K_f\right) \tag{3}$$

From (2) and (3), it can be seen that the torque is inversely proportional to the air-gap length and the suspending force is inversely proportional to the square of the air-gap length. Thus, any decrease in air-gap results in an increase in the electromagnetic torque and suspending force, vice versa.

III. ECCENTRICITY ANALYSIS OF 12/14 BLSRM

As is generally known, the rotor of the proposed BLSRM cannot be supported by mechanical bearings. So, the center position of the rotor can suffer displacement and eccentricity effects caused by a disturbance load and force. However, the maximum rotor eccentricity is restricted by the capture bearing at *g/2*. Fig. 3 shows the possible rotor eccentricity in the proposed BLSRM. The output torque and suspending forces of the torque and suspending force winding can be changed according to the air gap displacements.

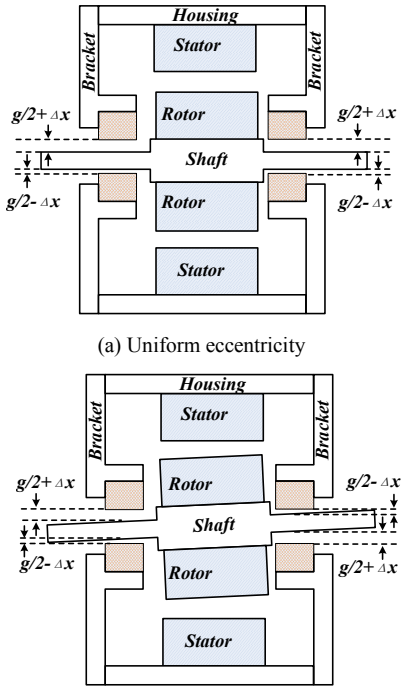

Figure 3. Rotor eccentricity in 12/14 BLSRM.

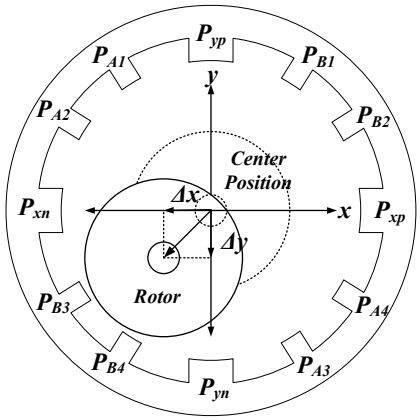

Figure 4. Uniform eccentricity of rotor in 12/14 BLSRM.

To get the eccentricity characteristics of the proposed structure, such as torque and suspending force, the proposed structure is analyzed by the software MATLAB combined with the FEA software, finite element method magnetics (FEMM).

A. Torque Characteristics

Fig. 4 shows the air-gap displacement according to the rotor eccentricity. When the rotor has eccentricity displacement in the negative x-direction, the output torques of the torque and suspending force winding with a constant value for various eccentric displacements are shown in Fig. 5. As shown in Fig. 5 (a), the peak value of the output torque increases slightly according to the rotor eccentricity. It is because the air gap distribution changes with the rotor eccentricity. That is, the air gap between stator poles P_{A1}, P_{A2} and the rotor is decreased, while the air gap between stator

poles P_{A3}, P_{A4} and the rotor is increased. According to (2), it can be known that the torque generated by the windings on stator poles P_{A1} and P_{A2} increases and decreases under the stator pole P_{A3} and P_{A4}. However, the amount of increase in the torque generated by the windings on stator poles P_{A1}, P_{A2} is greater than that of decrease in the toque generated by the windings on stator poles P_{A3}, P_{A4}. Hence, the total torque will be increased.

For instance, when the rotor is in normal position, the air gap is g, the torque generated by the windings on stator poles P_{A1} and P_{A2} is equal to T and the torque generated by the windings on stator poles P_{A3} and P_{A4} is equal to T. Accordingly, the total torque is $2T$. When the rotor has a eccentricity of $g/2$ towards the center of the negative x-direction and the positive y-direction, the air-gap between stator poles P_{A1}, P_{A2} and the rotor is $g/2$, and the air-gap between stator poles P_{A3}, P_{A4} and rotor is the $3g/2$, so that if ignore the effect of saturation and fringing flux, according to (2), it can be found that the torque generated by the windings on stator poles P_{A1} and P_{A2} is $2T$, while the torque generated by the windings on stator poles P_{A3} and P_{A4} is $2T/3$. Accordingly, the total torque is $8T/3$, which is larger than $2T$. Therefore, the total torque is increased.

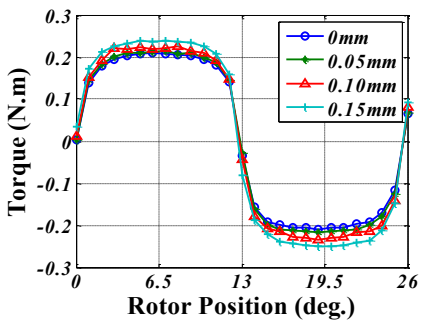

(a) Torque of torque winding at i_A=2A.

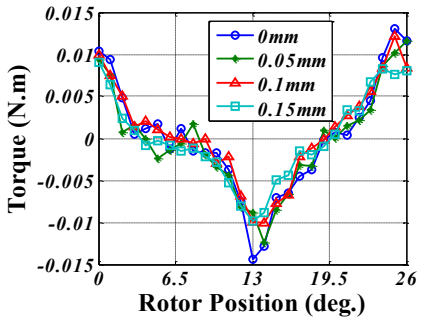

(b) Torque of suspending force winding at i_{xp}=2A.

Figure 5. Torque characteristics of 12/14 BLSRM for various rotor eccentric displacements (Δx).

Fig. 5 (b) shows the torque profiles with fixed suspending force current (i_{yp}=2A) at different eccentricities in the negative x-direction. As shown in Fig. 5 (b), the variation and peak value of the torque generated by the suspending force winding is much smaller than that generated by the torque winding. This is because the pole arc of the suspending force pole is not smaller than one rotor pole pitch, for the cause of the proposed BLSRM. Although the air-gap distribution changes with rotor eccentricity, the overlap area between suspending force pole and rotor pole is constant. Accordingly, the slope of the inductance with respect to rotor position is zero. Therefore, the torque control can be decoupled from suspending force control in the proposed structure.

B. Suspending Force Characteristics

Fig. 6 shows the suspending force generated by the torque winding with a constant current for different eccentricities in the negative x-direction. Unlike the rotor in the center position, in which the suspending force is almost zero, the suspending force generated by the torque winding is very large with different eccentricities. Moreover, with the eccentricity displacement increasing, the suspending force is also increased. It is because the air-gap between stator poles P_{A1}, P_{A2} and the rotor is decreased, while the air-gap between stator poles P_{A3}, P_{A4} and the rotor is increased. According to (3), it can be known that, compared with the suspending force generated in normal air-gap, the suspending force generated by the windings on stator poles P_{A1} and P_{A2} is increased due to the deceased air-gap, and the suspending force generated by the windings on stator poles P_{A3} and P_{A4} is decreased due to the increased air-gap. Therefore, an unbalance pull force will be generated by the torque windings along the direction towards the center of stator poles P_{A1} and P_{A2}. This force can be divided into two forces: one along the negative x-direction; the other along the positive y-direction.

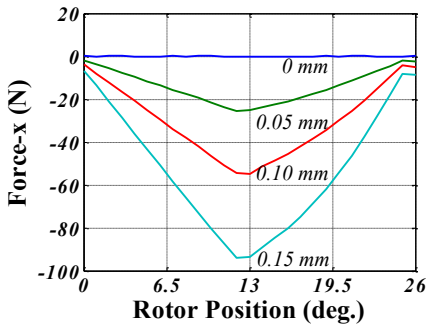

(a) Suspending force (F_x) of torque winding.

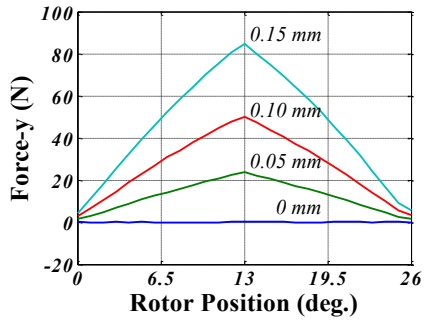

(b) Suspending force (F_y) of torque winding.

Figure 6. Suspending force chacracteristics of 12/14 BLSRM for various rotor eccentric displacements (Δx) with fixed torque winding current (i_A=2A).

Fig. 7 shows the suspending force generated by the suspending force pole P_{xp} with different eccentricities in the negative x-direction. It can be seen that the value of the suspending force in the x-direction decreases with increasing

eccentricity, which can also be explained by (3). Compared with Fig. 6, it can be found that, although the value of the suspending force is decreased, the suspending force generated by the suspending force winding is still larger than the unbalance force generated by the torque windings when the rotor has eccentricity displacement 0.15mm. That is, the rotor can be pulled back to the center position with rotor eccentricity smaller than 0.15mm.

If the rotor eccentricity is larger than 0.15mm, the motor may cannot generate enough force to pull the rotor back to the center position, which makes the suspension failed. This is the reason why the capture bearing is used to limit the maximum eccentricity of the rotor at 0.15mm.

IV. Simulation Analysis of 12/14 BLSRM

According to the operation principle of the proposed BLSRM, a control scheme for proposed BLSRM is proposed in Fig. 8. As shown in Fig. 8, mathematical model is not used, only a PI type speed controller is adopted to regulate the motor speed, and two independent close-loop PID air-gap displacement controllers, one for x-direction and the other for y-direction, are used to generate the desired suspending force commands F_x^* and F_y^* to keep the rotor at the center position. Further, in the control scheme, the command currents, i_x^* and i_y^*, for which suspending force windings are determined by Table I according to the desired radial force. Meanwhile, the hysteresis current control method is used to regulate the current in each phase.

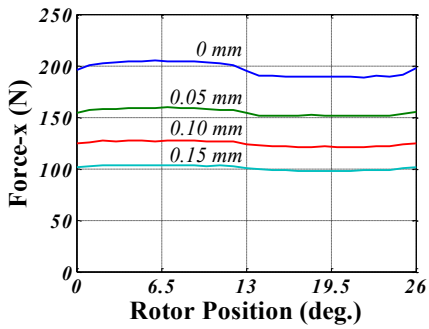

Figure 7. Suspending force chacracteristics with fixed suspending force current (i_{xp}=4A) at various eccentricities in negative x-direction.

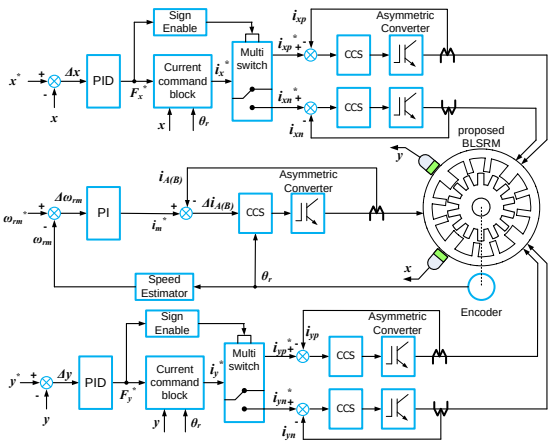

Figure 8. Control Scheme of 12/14 BLSRM.

TABLE I. Selection of Suspending Force Control Poles

Desired force	Suspending force control pole
$F_x>0$ & $F_y>0$	P_{xp} & P_{yp}
$F_x>0$ & $F_y<0$	P_{xp} & P_{yn}
$F_x<0$ & $F_y>0$	P_{xn} & P_{yp}
$F_x<0$ & $F_y<0$	P_{xn} & P_{yn}

According to the control scheme of the proposed BLSRM, simulations are performed to analyze the dynamic characteristics of 12/14 BLSRM. The simulations are divided into three steps. Firstly, the rotor is locked and suspended to the center position. Secondly, while the rotor is being steadily suspended, a torque load is applied to the rotor shaft, and torque currents are injected to accelerate the rotor to the desired speed. Finally, while the rotor is being steadily suspended and steadily operates at the desired speed, loads of suspending force is suddenly changed and the characteristics of the proposed structure are observed.

Assume the following initial conditions: two 10N loads are applied to the rotor shaft in the x- and y-directions simultaneously. Meanwhile, in the x-direction, the initial rotor eccentricity displacement is -120μm, and in the y-direction, initial rotor eccentricity displacement is -90μm.

Fig. 9 shows the simulation results of 12/14 BLSRM. It can be seen from Fig. 9 that, when suspension control is applied, the suspending force windings on the suspending force poles P_{xp} and P_{yp} are excited according to Table I. Accordingly, the suspending forces are generated as shown in Fig. 9 (g) and (h). From Fig. 9 (c) and (d), it can be seen that, when the suspension control is applied, eccentric errors in the two directions can be rapidly reduced to zero, which means that the rotor can be kept in the center position.

While the rotor is being steadily suspended, a 0.25N.m torque load is applied to the rotor shaft at the time t=0.1 second, and then the torque currents are injected to accelerate the rotor to the desired speed, 1000rpm. As shown in Fig. 9, with the torque winding currents and motor speed increasing, the rotor can still be steadily suspended, and the suspending force winding currents and suspending force generated by the suspending force winding are almost same as before. That is, when the rotor in the center position, the torque current has almost no effect on the suspending force, which has a good match with the analysis results shown in [10].

When the rotor is being steadily suspended at 1000rpm, a suspending force load in the x-direction is suddenly increased from 10N to 30N at the time t=0.2 second. As shown in Fig. 9 (c), the rotor has a little eccentricity in x-direction when the suspending force load is increased from 10N to 30N, but it can be pulled back to the center position with suitable suspending force control. Meanwhile, from Fig. 9 (g) and (h), it can be found that, when the rotor has eccentricity, the torque winding will generate radial force. And the radial force is decreased with decreased eccentricity. To steadily suspend the rotor in the center, the suspending force currents have to be changed to generate the suspending force to compensate the radial force generated by the torque windings. Further, with the rotor eccentricity and change of suspending force currents, the speed and phase current are almost same as before, which has a good match with the analysis results in Section III.

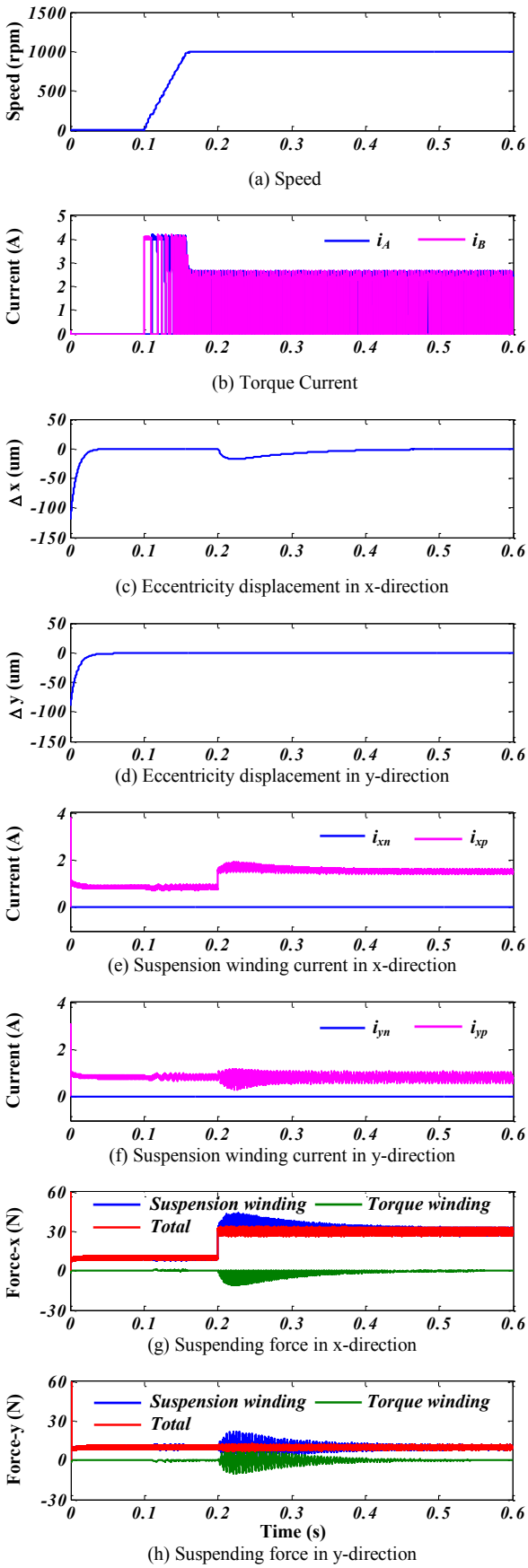

Figure 9. Simulation results of 12/14 BLSRM.

When the rotor is pulled back to the center position again, there is almost no radial force generated by the torque windings. However, compared with the radial force current before suspending force load change, the current in the y-direction has larger fluctuation than before. It is caused by the coupling effect of the radial force current in the x-direction.

The simulation results verify the correctness of the analysis results in [10] and Section III. It also verifies that the torque control can be decoupled from the suspending force control in 12/14 BLSRM.

V. Efficiency Estimation of 12/14 BLSRM

To further verify the validity of the proposed structure, efficiency estimation is executed to the 8/10 and proposed BLSRM.

A. Copper Loss

The copper loss is proportional to the square of the phase RMS current and phase winding resistance. Hence, according to the current waveform, the copper loss can be calculated as,

$$P_{cu} = mI_{phrms}^2 R_{ph} \tag{4}$$

$$I_{phrms} = \sqrt{\frac{1}{T}\int_0^T I_m^2 dt} \tag{5}$$

where, m is the number of phase, I_{phrms} is the RMS current of phase, R_{ph} is the phase resistance, T is the time of one period, I_m is the phase current.

B. Core Loss

The core loss is composed of hysteresis loss, excessive loss and eddy-current loss. It can be calculated as,

$$P_{losses}(t) = P_h(t) + P_c(t) + P_e(t) \tag{6}$$

where,

$$P_h(t) = \left\{ \left| H_x \frac{dB_x}{dt} \right|^{\frac{2}{\beta}} + \left| H_y \frac{dB_y}{dt} \right|^{\frac{2}{\beta}} \right\} \tag{7}$$

$$P_e(t) = \frac{1}{C_e} k_e \left\{ \left| \frac{dB_x}{dt} \right|^2 + \left| \frac{dB_y}{dt} \right|^2 \right\}^{0.75} \tag{8}$$

$$P_c(t) = \frac{1}{2\pi^2} k_c \left\{ \left| \frac{dB_x}{dt} \right|^2 + \left| \frac{dB_y}{dt} \right|^2 \right\} \tag{9}$$

in which, P_h, P_c and P_e are the hysteresis loss, excessive loss, and eddy-current loss, respectively; k_h, k_e and k_c are the coefficient of hysteresis loss, excessive loss, and eddy-current loss, respectively. According to the material of the prototypes, the lamination steel 35PN440 is used as the stator and rotor material in the analysis. From the datasheet, k_h, k_e and k_c are given as 270.39764, 4.30046 and 0.30463 W/m^3, respectively.

C. *Simulation Results*

An external circuit is built and used to drive the two motors operating at rated condition. Meanwhile, hysteresis current control method is used to regulate the phase current. Figs. 10 and 11 show the transient phase current and core loss in the two motors. Compared with Figs. 10 (a) and 11 (a), it can be seen that the core losses are mainly produced at commutation region. Further, compared with core loss in 8/10 type, the core loss in 12/14 type is much smaller due to the short flux path and no flux reversal in this structure.

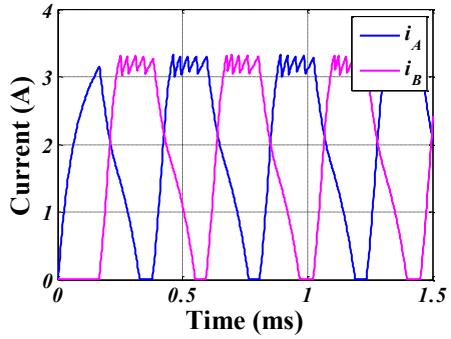

Figure 10. Phase current of 12/14 BLSRM operating at rated condition.

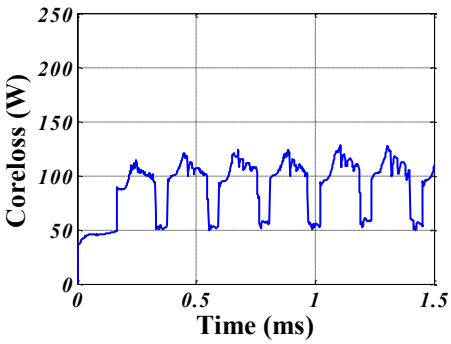

(a) 12/14 BLSRM

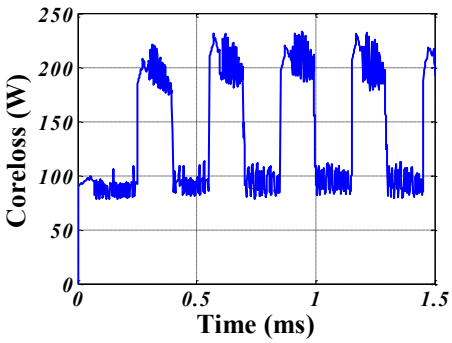

(b) 8/10 BLSRM

Figure 11. Core loss of 12/14 and 8/10 BLSRMs operating at rated condition

According to Section V.A and Fig. 10, the copper loss of 12/14 BLSRM can be calculated. Table II shows the estimated efficiency of 8/10 and 12/14 BLSRM. From Table II, it can be seen that the core loss of the 8/10 type is larger than the proposed type, it is because long flux and flux reversal exist in the flux path of the 8/10 type. Further, the output power and efficiency of the proposed type is larger than that in the 8/10 type, which further verifies the effectiveness of the 12/14 BLSRM.

TABLE II. ESTIMATED EFFICIENCY OF 8/10 AND PROPOSED BLSRM

Parameter		Value	
		8/10 type	Proposed type
P_{cu_T}	Copper loss	15.54 W	20.5W
P_{Fe}	Core loss	148.93 W	95.63 W
P_{out}	Output power	355.70 W	415.47 W
η	Efficiency	68.38%	78.15%

VI. CONCLUSIONS

In this paper, the rotor eccentricity effect in the proposed BLSRM is analyzed. Based on the analysis results, the torque control can be decoupled from the suspending force control. Although the unbalance force generated by the torque winding is very large due to the rotor eccentricity, enough suspending force can be generated by the suspending force to pull the rotor back to the center positions. Moreover, due to short flux and no flux reversal in the stator, the efficiency of the proposed type is higher than 8/10 type.

ACKNOWLEGEMENT

This work was supported by the Ministry of Education (MOE) and National Research Foundation of Korea (NRF) though BK21 plus project.

REFERENCES

[1] D. H. Lee and J. W. Ahn, "Design and analysis of hybrid stator bearingless SRM," *Journal of Electrical Engineerig & Technology*, vol. 6, no. 1, pp. 94-103, 2011.

[2] D. H. Lee, T. H. Pham and J. W. Ahn, "Design and operation characteristics of four-two pole high-speed SRM for torque ripple reduction," *IEEE Transaction on Industrial Electronics*, vol. 60, no. 9, pp. 3637-3643, 2013.

[3] M. Takemoto, H. Suzuki, A. Chiba, T. Fukao, M. A. Rahman, "Improved analysis of a bearingless switched reluctance motor," *IEEE Transaction on Industrial Application*, vol. 37, no. 1, pp. 26-34, 2001.

[4] M. Takemoto, A. Chiba, H. Akagi, and T. Fukao, "Radial force and torque of a bearingless switched reluctance motor operating in a region of magnetic saturation," *in Conf. Record IEEE-IAS Annual Meeting*, 2002, pp. 35–42.

[5] M. Takemoto, A. Chiba, H. Akagi, and T. Fukao, "Radial force and torque of a bearingless switched reluctance motor operating in a region of magnetic saturation," *IEEE Transaction on Industry Applications*, vol. 40, no. 1, pp. 103-112, 2004.

[6] F. C. Lin and S. M. Yang, "Self-bearing control of a switched reluctance motor using sinusoidal currents," *IEEE Transaction on Power Electroics.*, vol. 22, no. 6, pp. 2518-2526, 2007.

[7] L. Chen and W. Hofmann, "Modeling and control of one bearingless 8-6 switched reluctance motor with single layer of winding structure," in *Proc. of the 2011-14th European Conference on Power Electronics and Applications (EPE 2011)*, Aug. 30-Sep. 1, 2011.

[8] L. Chen and W. Hofmann, "Speed regulation technique of one bearingless 8/6 switched reluctance motor with simpler single winding structure," *IEEE Transactions on Industrial Electronics*, vol. 59, no. 6, pp. 2592-2600, 2012.

[9] Carlos R. Morrison, Mark W. Siebert, and Eric J Ho, "Electromagnetic forces in a hybrid magnetic-bearing switched-reluctance motor," *IEEE Transactions on Magnetics*, vol.44, no.12, 2008.

[10] Z. Y. Xu, F. G. Zhang, and J. W. Ahn, "Design and analysis of a novel 12/14 hybrid pole type bearingless switched reluctance motor," *Proceedings on International Symposium on Industrial Electronics*, pp. 1922-1927, 2012.